Tension-dependent nucleosome remodeling at the pericentromere in yeast

Jolien S. Verdaasdonk, Ryan Gardner, Andrew D. Stephens, Elaine Yeh, and Kerry Bloom
Department of Biology, University of North Carolina at Chapel Hill, Chapel Hill, NC 27599

ABSTRACT Nucleosome positioning is important for the structural integrity of chromosomes. During metaphase the mitotic spindle exerts physical force on pericentromeric chromatin. The cell must adjust the pericentromeric chromatin to accommodate the changing tension resulting from microtubule dynamics to maintain a stable metaphase spindle. Here we examine the effects of spindle-based tension on nucleosome dynamics by measuring the histone turnover of the chromosome arm and the pericentromere during metaphase in the budding yeast *Saccharomyces cerevisiae*. We find that both histones H2B and H4 exhibit greater turnover in the pericentromere during metaphase. Loss of spindle-based tension by treatment with the microtubule-depolymerizing drug nocodazole or compromising kinetochore function results in reduced histone turnover in the pericentromere. Pericentromeric histone dynamics are influenced by the chromatin-remodeling activities of *STH1/NPS1* and *ISW2*. Sth1p is the ATPase component of the Remodels the Structure of Chromatin (RSC) complex, and Isw2p is an ATP-dependent DNA translocase member of the Imitation Switch (ISWI) subfamily of chromatin-remodeling factors. The balance between displacement and insertion of pericentromeric histones provides a mechanism to accommodate spindle-based tension while maintaining proper chromatin packaging during mitosis.

INTRODUCTION

Nucleosomes form the basis for packaging of DNA into chromatin. Two copies each of histones H2A, H2B, H3, and H4 are wrapped by 145–147 base pairs of DNA (Luger *et al.*, 1997). Histone protein levels are tightly regulated, as both overexpression and depletion have deleterious effects, including disruption of nucleosome organization surrounding the centromere (Saunders *et al.*, 1990). Histone genes are transcribed and the protein incorporated during DNA replication. Histone deposition is believed to occur in a stepwise manner, with H3–H4 tetramers bound first, followed by two H2A–H2B dimers (Verreault, 2000; Akey and Luger, 2003). Histone eviction has been proposed to occur in reverse, with H2A/H2B being more mobile than H3/H4 (Kimura and Cook, 2001; Jamai *et al.*, 2007). Outside of replication-dependent histone incorporation, histones are known to be dynamic during transcription in a manner dependent on RNA polymerase II (Widmer *et al.*, 1984; Lee *et al.*, 2004; Chen *et al.*, 2005; Kimura, 2005; Thiriet and Hayes, 2005; Dion *et al.*, 2007; Kim *et al.*, 2007; Deal *et al.*, 2010; Lopes da Rosa *et al.*, 2011).

Individual histones display different dynamic properties within actively transcribed or silent regions. Histone H2B is dynamic at both active and inactive loci, whereas histone H3 is dynamic predominantly at active loci (Pusarla and Bhargava, 2005; Jamai *et al.*, 2007). Histone H3 displays rapid exchange at highly transcribed regions, such as rRNA gene loci, associated with the incorporation of an H3 variant (Ahmad and Henikoff, 2002; Thiriet and Hayes, 2005; Lopes da Rosa *et al.*, 2011). Histones are stable during metaphase in HeLa cells when transcription is silenced, and when transcription resumes upon anaphase onset histones are found to be more dynamic (Chen *et al.*, 2005). Similarly, histones are exchanged during a single cell cycle in yeast (Cho *et al.*, 1998; Schwabish and Struhl, 2004).

Histone dynamics are regulated by ATP-dependent chromatin-remodeling complexes, which in budding yeast include the Imitation Switch (ISWI) and switching defective 2/sucrose nonfermenting 2 (SWI2/SNF2; SWI/SNF and Remodels the Structure of Chromatin [RSC]) families of chromatin remodelers (Clapier and Cairns, 2009). The ISWI family is known to remodel nucleosomes as well as function

as a chromatin assembly factor (Corona *et al.*, 1999). Isw2p is the nucleosome-stimulated ATPase of the ISW2 complex in the ISWI family of chromatin remodelers that exhibits nucleosome-spacing activities resulting in increased nucleosome occupancy (Tsukiyama *et al.*, 1999; Flaus and Owen-Hughes, 2003; Whitehouse *et al.*, 2003, 2007). Isw2p is located throughout the nucleus in budding yeast (Supplemental Figure S1). Antagonistic activities of ISW2 and SWI/SNF control gene expression; ISW2 increases nucleosome occupancy to exclude SWI/SNF and silence gene expression (Tomar *et al.*, 2009). The yeast SWI/SNF and RSC remodeling complexes contain the conserved homologous ATPase subunits Swi2p/Snf2p and Sth1p/Nps1p, respectively (Tsuchiya *et al.*, 1992; Cairns *et al.*, 1996; Du *et al.*, 1998; Vignali *et al.*, 2000). Sth1p/Nps1p demonstrates DNA-dependent ATPase activity resulting in the eviction of nucleosomes (Lorch *et al.*, 2006; Chaban *et al.*, 2008; Parnell *et al.*, 2008; Erkina *et al.*, 2010), is essential for mitotic growth (Cairns *et al.*, 1996; Cao *et al.*, 1997; Tsuchiya *et al.*, 1998; Xue *et al.*, 2000; Saha *et al.*, 2002), and is located throughout the nucleus (Supplemental Figure S1).

RSC is required for chromatin organization in the pericentromere and kinetochore structure in budding yeast (Tsuchiya *et al.*, 1998; Hsu *et al.*, 2003). Loss of Sth1p/Nps1p function results in reduced histone occupancy around the centromere by nucleosome-scanning assay and chromatin immunoprecipitation (Desai *et al.*, 2009) and leads to cell cycle arrest at G2/M. Nucleosomes flanking the centromere are subject to disruptive tension from the spindle, which would require removing mislocalized nucleosomes and reloading them in the proper position. In the absence of nucleosome removal (i.e., loss of RSC), the nucleosomes flanking the centromere cannot be efficiently repositioned and become disorganized, and the net effect is reduced overall occupancy (Desai *et al.*, 2009).

The pericentromere is approximately 50 kb of chromatin flanking the centromere forming a C-loop (Yeh *et al.*, 2008). This chromatin is located in a defined region in metaphase cells (~800 × ~300 nm cylinder between the spindle pole bodies; Figure 1A), corresponding to the region enriched for cohesin and condensin (Yeh *et al.*, 2008; Stephens *et al.*, 2011). The pericentromeric chromatin acts as an elastic spring to balance the outward forces exerted by the mitotic spindle in metaphase (Bouck and Bloom, 2007; Stephens *et al.*, 2011). To determine the contribution of histone dynamics in packaging and maintaining the metaphase chromatin spring, we measured histone turnover within the pericentromere and its regulation by ATP-dependent chromatin-remodeling factors. We show that regulation of histone dynamics by chromatin remodelers is important for kinetochore structure, pericentromeric chromatin organization, and metaphase spindle length.

RESULTS

Histone dynamics differ in the pericentromere and chromosome arm during metaphase

We determined the dynamics of histones H2B and H4 in the pericentromere and the chromosome arm during metaphase in *Saccharomyces cerevisiae* by measuring the half-life ($t_{1/2}$) of fluorescence recovery after photobleaching (FRAP). Strains containing histone tagged with green fluorescent protein (GFP) and spindle pole bodies tagged with red fluorescent protein (RFP; see Table 1 in *Materials and Methods*) allowed us to demarcate the pericentromere from chromosomal arms in a living cell. The pericentromere lies between the spindle pole bodies (Yeh *et al.*, 2008), and the chromosome arms are distal to the spindle (Figure 1).

Histones within the pericentromere exhibit faster turnover rates than in the chromosome arms. Histone H2B has a $t_{1/2}$ of 62 s in the pericentromere during metaphase, compared with 87 s in the arm (Figures 1B and 2A and Supplemental Table S1). Histone H4 has a $t_{1/2}$ of 76 s in the pericentromere, compared with 121 s in the chromosome arm (Figures 1C and 2A and Supplemental Table S2). H2B is more dynamic than H4 in both regions of the chromosome. For both H2B and H4, the $t_{1/2}$ values of the chromosome arm are significantly slower than those of the pericentromere (Student's *t* test, p < 0.05). The final percentage recoveries of histone protein were found to be similar for both regions and histones measured, indicating similar levels of mobile protein (Figure 2B and Supplemental Tables S1 and S2). The individual dynamics of H2B and H4 both within the pericentromere and the arms are consistent with the observations that each histone pair, H2A/H2B and H3/H4, is independently regulated (Jackson, 1987; Smith and Stillman, 1991; Ladoux *et al.*, 2000; Akey and Luger, 2003; Jin *et al.*, 2005; Thiriet and Hayes, 2005).

Histone dynamics in the pericentromere are reduced on loss of spindle-based tension

To determine whether histone dynamics in the pericentromere were influenced by spindle-based tension, we treated cells with the microtubule-depolymerizing drug nocodazole (noc) and examined histone half-life. In nocodazole-arrested cells, the spindle pole bodies collapse into a single diffraction-limited spot and the pericentromeric chromatin remains adjacent to the spindle pole bodies. On photobleaching, we observed two populations of histone recovery. There was a significant reduction in the number of cells with measurable H4 recovery dynamics in the pericentromere, with the chromosome arm largely unaffected (pericentromere, 92% untreated wild type (WT) vs. 55% noc treated; arm, 97% untreated WT vs. 85% noc treated; Fisher's exact test, p < 0.05; Figure 3A). H2B also showed a decrease in cells exhibiting measurable dynamics (pericentromere, 92% untreated WT vs. 74% noc treated; arm, 100% untreated WT vs. 83% noc treated), but these were not found to be statistically significant (Fisher's exact test, p < 0.05; Figure 3A).

When histone recovery was measurable, H2B half-life was significantly slowed in the pericentromere (62 s untreated WT vs. 121 s noc treated; Student's *t* test, p < 0.05; Figure 3B and Supplemental Table S1). There was no significant change in H2B recovery in the chromosome arm upon nocodazole treatment or any significant changes in final percentage recovery (Figure 3, B and C). Therefore, upon reduction of spindle tension by nocodazole treatment, the dynamics of pericentromeric H2B and H4 are reduced.

An alternative method to reduce pericentric tension was used by introducing a conditional allele of the kinetochore protein Nuf2 (Gal-*NUF2*). On galactose (gal) media the cells express *NUF2* and are able to assemble the kinetochore, whereas on glucose (glu) media *NUF2* expression is repressed compromising kinetochore function (Bouck and Bloom, 2005). Loss of Nuf2p resulted in reduced histone dynamics in the pericentromere but not the chromosome arm for both H2B and H4 (H2B: pericentromere, 62 s WT vs. 94 s Gal-*NUF2* on glu; arm, 87 s WT vs. 86 s Gal-*NUF2* on glu; H4: pericentromere, 76 s WT vs. 97 s Gal-*NUF2* on glu; arm, 121 s WT vs. 135 s Gal-*NUF2* on glu; Student's *t* test, p < 0.05; Figure 3B and Supplemental Tables S1 and S2). The final percentage recovery of H2B was not significantly affected, whereas the final percentage recovery of H4 in the pericentromere was significantly reduced (64% WT vs. 30% Gal-*NUF2* on glu; Figure 3C), indicating a reduced level of mobile histones. Thus, like nocodazole treatment, the loss of spindle tension via reduction of kinetochore function results in significantly reduced histone dynamics in the pericentromere and not in the chromosome arm.
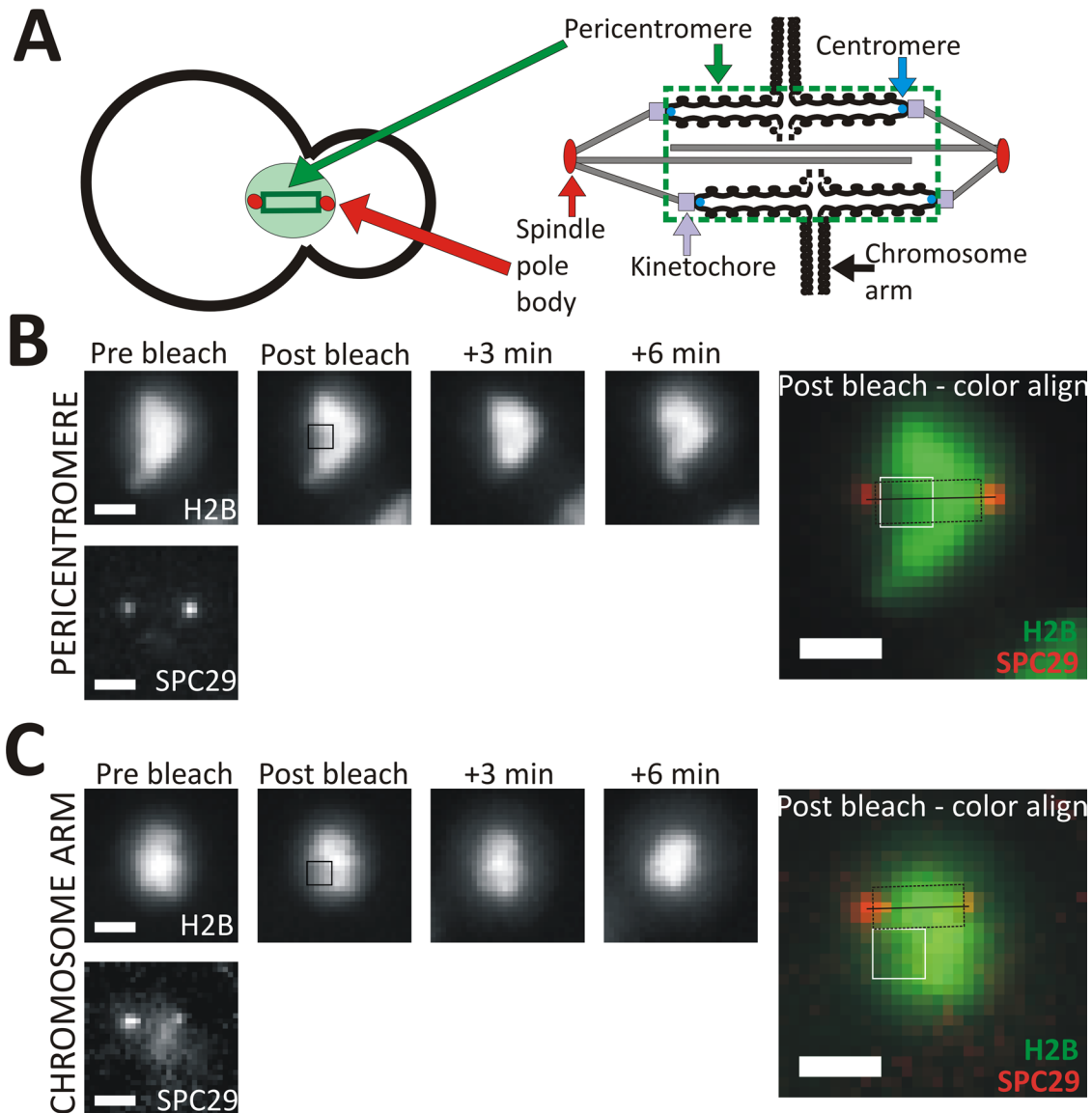
FIGURE 1: In vivo photobleaching of the pericentromere and chromosome arm, using spindle pole bodies as fiduciary markers. (A) Diagram showing the organization of the pericentromeric chromatin in budding yeast (Yeh *et al.*, 2008). The pericentromere is defined by the region of cohesin enrichment between the spindle pole bodies. (B, C) Representative images of FRAP experiments in the pericentromere (B) and chromosome arm (C). Shown is the histone-GFP signal before photobleaching, postphotobleaching (with bleached area outlined by black square), 3 min postphotobleaching, and 6 min postphotobleaching. The color align image shows the spindle pole bodies (Spc29p-RFP) relative to the postphotobleaching H2B-GFP, with location of bleaching denoted by the 5 × 5 pixel white square. The spindle axis (solid black line) and the pericentromere (dotted black line) are shown in relation to the photobleached spot. Bar, 1 μm.

Increased histone dynamics are the result of increased histone removal

At least two properties of histone dynamics can contribute to the observed behavior in the pericentromere: either the histones are removed from DNA more frequently in the pericentromere, or histones are replaced more quickly, leaving binding sites in the arm unbound longer. To address these possible explanations, we examined the dynamics of H2B tagged with a photoactivatable GFP (paGFP) fluorophore (Vorvis *et al.*, 2008).

The highly dynamic nature of proteins can be visualized using photoactivation (Figure 4A). As a control, we examined the dispersion characteristics of photoactivated Erg6p, a membrane protein involved in ergosterol biosynthesis (Gaber *et al.*, 1989; Vorvis *et al.*,

2008). Erg6p exhibited dispersion in all of the examined cells, indicative of a high level of dynamics (Figure 4B and Supplemental Table S3). Dispersion was measured by quantifying the loss of signal intensity in a 2.6 × 2.6 μm area over time (20 × 20 pixels; *Materials and Methods*). Photoactivation of H2B in the pericentromere and chromosome arm reveals that the percentage of cells showing histone dispersion is not significantly different in the pericentromere and the chromosome arm (79 vs. 83%, respectively; Fisher's exact test, p < 0.05; Figure 4B). The removal dynamics of histone protein are not different in the pericentromere and chromosome arm. Therefore the increased histone dynamics observed by FRAP in the pericentromere under tension are likely the result of active processes replacing lost histones more rapidly.
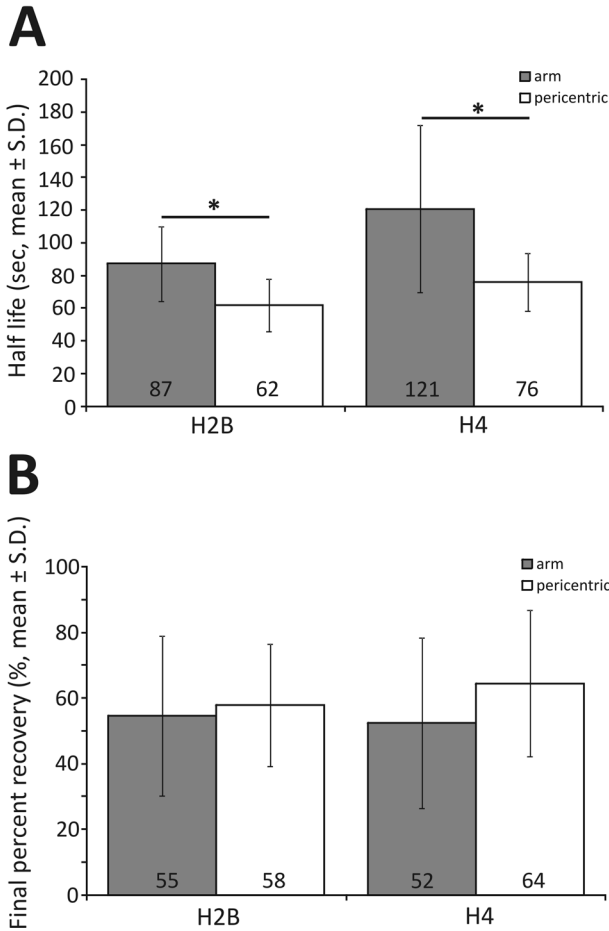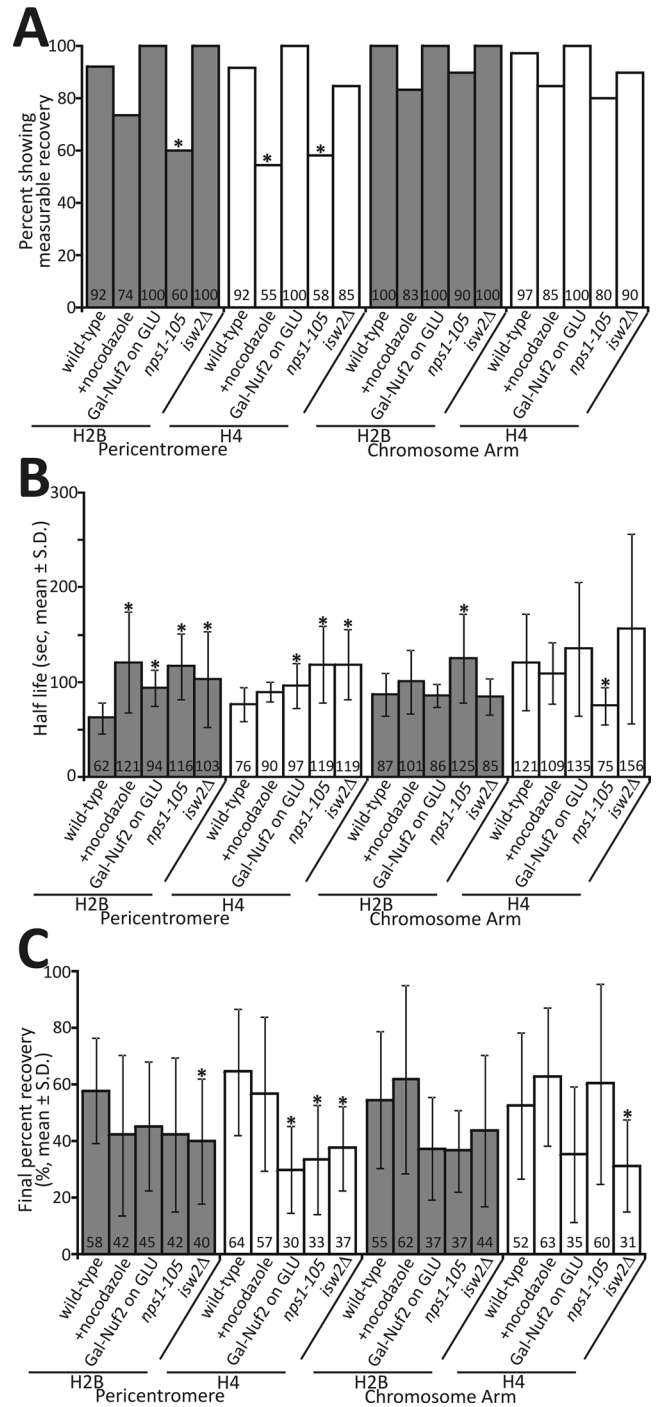
FIGURE 2: Histones in the pericentromere are more dynamic than those of the chromosome arm. (A) Graph of average half-life in seconds measured by FRAP for histones H2B and H4 in the pericentromere and chromosome arm. Asterisks indicate statistically significant differences (Student's t test, p < 0.05) between arm and pericentromere regions for each histone. All data are summarized in Supplemental Tables S1 (H2B) and S2 (H4). Normalized FRAP recovery curves are shown in Supplemental Figure S2. (B) Graph of final percentage recovery of histone fluorescence signal after photobleaching. Final percentage recovery reflects the amount of mobile protein that exhibited fluorescence recovery. These values are not statistically significantly different (Student's t test, p < 0.05). Graph, mean ± SD.

Loss of spindle tension leads to a significant decrease in the percentage of cells displaying dispersion of photoactivated H2B in the pericentromere but not the chromosome arm (pericentromere, 79% untreated WT vs. 33% noc treated; arm, 83% untreated WT vs. 46% noc treated; Fisher's exact test, p < 0.05; Figure 4B). The reduced histone dispersion in the pericentromere in collapsed spindles points to reduced histone removal from the DNA in the absence of tension. The FRAP and photoactivation data indicate an active histone replacement time under tension and an increased histone dwell time (slower off rate) in the pericentromere upon loss of spindle tension.

Loss of Sth1p/Nps1p or Isw2p leads to reduced histone turnover in the pericentromere

To address whether chromatin remodelers are involved in nucleosome exchange at the pericentromere, we measured histone dynamics in

FIGURE 3: Loss of spindle tension or chromatin-remodeling activity results in reduced histone dynamics primarily at the pericentromere. (A) Graph showing percentage of samples showing measurable recovery after photobleaching. Samples whose final percentage recovery was >0% were defined as not showing measurable recovery. Asterisks indicate statistically significant differences between sample and corresponding wild-type value (Fisher's exact test, p < 0.05). (B) Graph of average histone half-life (seconds). *nps1-105* at permissive temperature (24°C). (C) Graph of final histone fluorescence percentage recovery, reflecting the mobile protein exhibiting recovery over the course of the time lapse. For both B and C, asterisks indicate statistically significant differences between sample and corresponding wild-type value (Student's t test, p < 0.05). All data (including sample sizes) are summarized in Supplemental Tables S1 (H2B) and S2 (H4). Graph, mean ± SD.
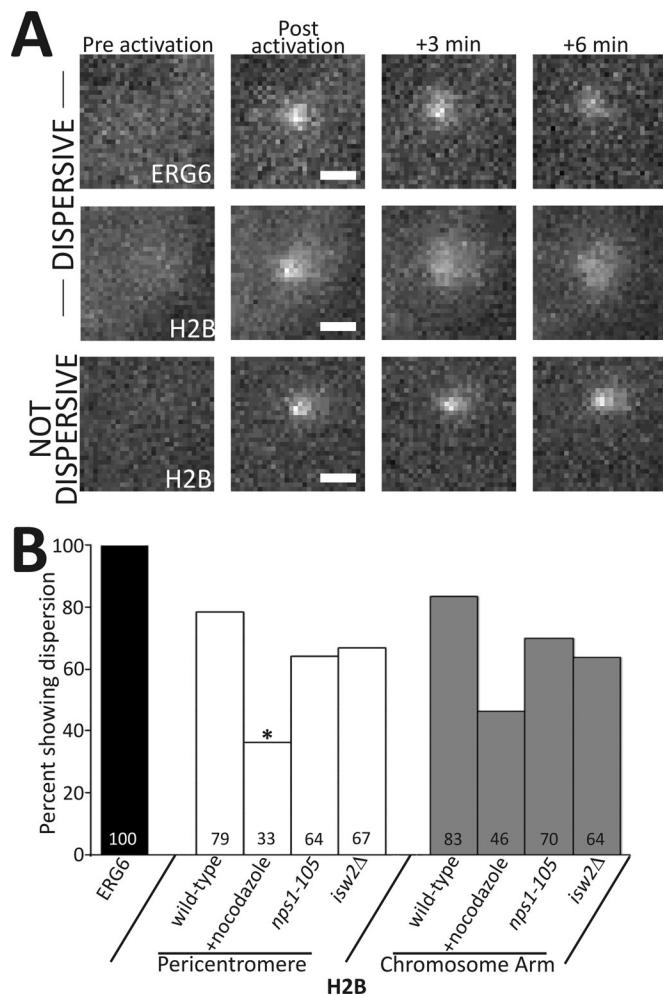
FIGURE 4: Loss of spindle tension results in reduced dispersal of photoactivated histone H2B. (A) Representative images showing nuclear region before photoactivation (preactivation), postphotoactivation, halfway through time lapse (+3 min), and at end of time lapse (+6 min). Top row, the dispersion of the control strain containing Erg6p-paGFP. Second and third rows, representative images of dispersive (row 2) and not dispersive (row 3) H2B-paGFP. Bar, 1 μm. (B) Percentage of cells showing dispersion of photoactivated Erg6p or H2B in the arm and pericentromere (wild-type = untreated, *nps1-105* at permissive temperature [24°C]). Dispersion is defined by the loss of fluorescence intensity over the course of the time lapse (*Materials and Methods*). Asterisks indicate statistically significant differences between sample and corresponding wild-type value (Fisher's exact test, *p* < 0.05; Supplemental Table S3). Percentage showing dispersion in the chromosome arm upon nocodazole treatment is approaching statistical significance (p < 0.1).

mutations in RSC (*STH1/NPS1*) and *ISW2*. In the absence of RSC activity (*nps1-105* temperature-sensitive allele), cells arrest in metaphase with defects in kinetochore assembly and segregation (Tsuchiya *et al.*, 1998; Hsu *et al.*, 2003). In the *nps1-105* mutant at permissive temperature (24°C), there is a significant decrease in the percentage of cells exhibiting measurable histone-GFP recovery in the pericentromere (H2B, 92% WT vs. 60% *nps1-105*; H4, 92% WT vs. 58% *nps1-105*; Fisher's exact test, p < 0.05; Figure 3A and Supplemental Tables S1 and S2). Of the cells with measurable histone recovery, the $t_{1/2}$ of H2B is significantly slowed as compared with wild type (pericentromere, 62 s WT vs. 116 s *nps1-105*; arm: 87 s WT vs. 125 s

nps1-105; Student's *t* test, p < 0.05, Figure 3B). The $t_{1/2}$ of H4 is also significantly altered in both the pericentromere and chromosome arm in *nps1-105* cells as compared with wild-type (pericentromere, 76 s WT vs. 119 s *nps1-105*; arm, 121 s WT vs. 75 s *nps1-105*; Student's *t* test, p < 0.05; Figure 3B). The final percentage recovery of histone H4 in *nps1-105* cells is significantly reduced from wild type in the pericentromere but unaffected in the chromosome arm (pericentromere, 64% WT vs. 33% *nps1-105*; arm, 52% WT vs. 60% *nps1-105*; Student's *t* test, p < 0.05; Figure 3C). Histone exchange in the pericentromere is dependent upon a fully functional RSC complex. When the photoactivatable H2B is used, the fraction of cells exhibiting dispersion is unchanged (Fisher's exact test, p < 0.05; Figure 4B). Thus histones are evicted in *nps1-105*, but the mechanisms replacing lost histones are diminished (Figure 3, A and B).

RSC chromatin remodeling during metaphase primarily affects the histone dynamics in the pericentromere, with histone dynamics in the chromosome arm affected to a lesser degree. The nucleus-wide alteration of histone dynamics is consistent with the essential nature of *STH1/NPS1*. However, histones in the pericentromere more often display no measurable recovery (Figure 3A), indicating a regional specificity for RSC chromatin-remodeling activity.

The requirement for antagonistic chromatin remodeling has been demonstrated at promoter regions to control expression levels (Tomar *et al.*, 2009; Erkina *et al.*, 2010). We reasoned that histone occupancy at the pericentromere might also reflect balanced chromatin remodeling. *ISW2* has been found to counter the histone removal activity of SWI/SNF chromatin remodeling (Tomar *et al.*, 2009).

In the absence of *ISW2* activity (*isw2Δ*), the $t_{1/2}$ of both histones H2B and H4 is significantly slower in the pericentromere but not the chromosome arm as compared with wild-type cells. H2B $t_{1/2}$ slows from 62 s in wild type to 103 in *isw2Δ* cells, and H4 $t_{1/2}$ slows from 76 s in wild-type cells to 119 s in *isw2Δ* cells (Student's *t* test, p < 0.05; Figure 3B and Supplemental Tables S1 and S2). Similarly, the final percentage recovery is significantly lower in the pericentromere but not the chromosome arm for both histones H2B and H4 (Student's *t* test, p < 0.05; Figure 3C). Wild-type H2B percentage recovery in the pericentromere is 58% and is reduced to 40% in *isw2Δ* cells. H4 percentage recovery in the pericentromere is 64% in wild-type cells and is reduced to 37% in *isw2Δ* cells. Consistent with the nonessential nature of *ISW2*, there is no significant difference in the percentage of cells showing measurable histone recovery between wild-type and *isw2Δ* cells (Fisher's exact test, p < 0.05; Figure 3A). As in the *nps1-105* cells, there was no significant change in percentage of cells exhibiting dispersion after photoactivation in *isw2Δ* cells as compared with wild type (Fisher's exact test, p < 0.05; Figure 4B). These data suggest that the primary role for *ISW2* is maintenance of nucleosome occupancy under tension by reloading histones rather than eviction, as there is no decrease in percentage of cells exhibiting measurable recovery (Figure 3A).

Chromatin packaging contributes to kinetochore organization

In yeast, the 16 kinetochores are clustered into a close-to-diffraction–limited spot. To address whether histone occupancy is important for this organization, we examined the structure of the inner (Ame1p-GFP or Ndc10p-GFP) and outer (Spc24p-GFP or Nuf2p-GFP) kinetochores (Figure 5, A and B). From this analysis, we observed significant disruption of the kinetochores in conditions that perturb chromatin packaging.

We first examined kinetochore structure upon the depletion of histone H3 and found that the inner, but not the outer (as in Bouck
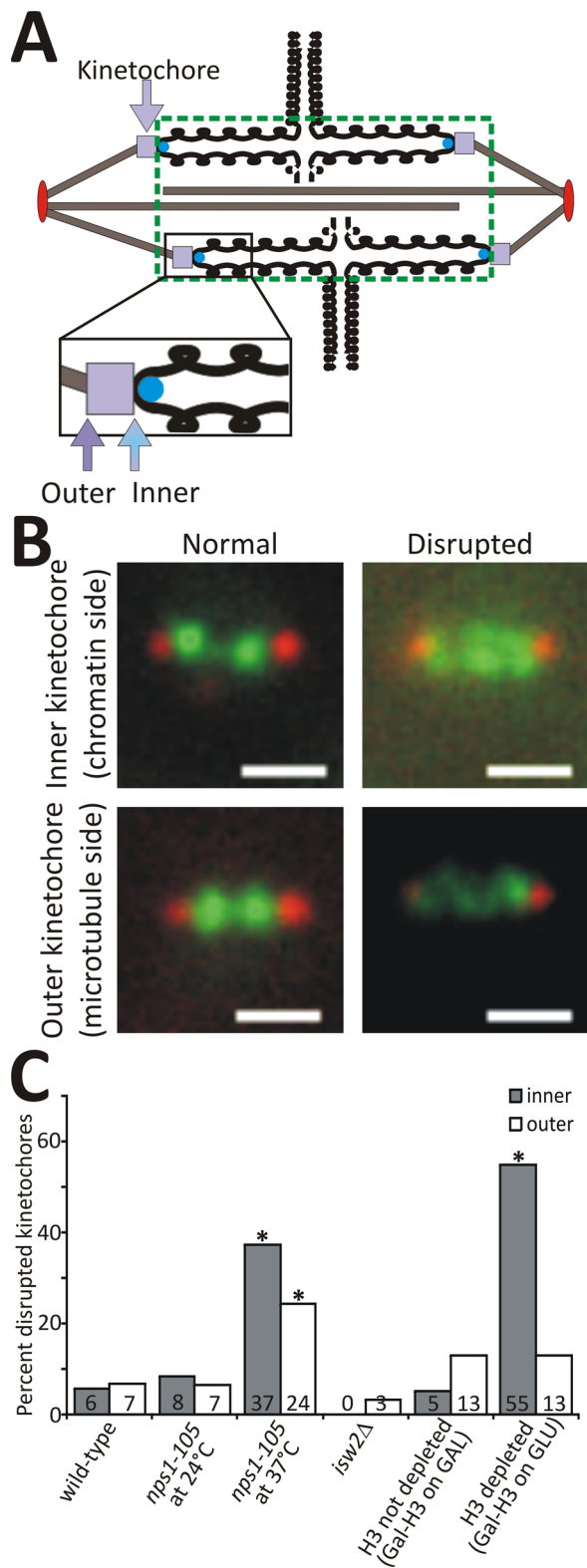
FIGURE 5: Disruption of the underlying chromatin platform results in disruption of the kinetochore. (A) Diagram of kinetochore location in relation to pericentromeric chromatin, as denoted by green dotted line. (B) Representative images of both normal and disrupted kinetochores. Either inner kinetochore (Ame1p-GFP) or outer kinetochore (Spc24p-GFP) is shown in green, and spindle pole bodies (Spc29p-RFP) are shown in red. Bar, 1 μm. (C) Graph showing percentage of kinetochores disrupted in single plane images. For wild-type cells, we imaged Ame1p-GFP for the inner kinetochore or

and Bloom, 2007), kinetochore is disrupted (Figure 5C and Supplemental Table S4). Cells expressing the sole copy of H3 under the galactose promoter exhibit disruption of the inner kinetochore (Ndc10p-GFP) in 5% of cells. On reduction of histone H3—resulting in an approximately twofold reduction in nucleosome concentration—55% of the cells show disruption of the inner kinetochore, a significant increase (Fisher's exact test, $p < 0.05$; Figure 5C). Decreasing histone density specifically affects the inner kinetochore organization, leaving the microtubule-binding components (Nuf2p-GFP) structurally intact. The significant disruption of the inner kinetochores observed in H3-repressed cells is not simply the disaggregation of the 16 individual kinetochores, because the outer kinetochore components remain properly organized. Thus the underlying pericentromeric chromatin contributes to the structure of the inner kinetochore and the correct linkage with the microtubule-binding outer kinetochore.

Loss of RSC function (*nps1-105* at restrictive temperature, 37°C) results in significant disruption of both the inner and outer kinetochores. The inner (Ame1p-GFP) and outer (Spc24p-GFP) kinetochores of *nps1-105* cells are disrupted 37 and 24%, respectively, as compared with 6 and 7% in wild-type cells (Fisher's exact test, $p < 0.05$; Figure 5C and Supplemental Table S4). The increase in disruption is more dramatic in the inner kinetochore (6% WT vs. 37% *nps1*-105), supporting the hypothesis that disruption of the underlying chromatin results in disrupted kinetochore organization. The disruption of the outer kinetochore (Spc24p-GFP) in *nps1-105* cells may suggest a role for RSC in kinetochore organization or stability. We did not observe increased kinetochore disruption in *isw2Δ* cells (Fisher's exact test, $p < 0.05$; Figure 5C). Thus nucleosome density and mobility within pericentromeric chromatin is essential in maintaining kinetochore structure.

DISCUSSION

Patterns of histone dynamics in metaphase

The proper organization of the pericentromere is essential for balancing spindle forces in metaphase, as well as for the attachment and alignment of sister chromatids. The work presented here provides a model for maintenance of histone occupancy in the pericentromere under tension through the balanced remodeling activities of RSC and ISW2 (Figure 6). The chromatin-remodeling activities of RSC and ISW2 are needed to maintain a balance of on and off rates of histones in the pericentromere. Loss of RSC activity (Figure 6D) results in reduced off rates (increased dwell time; Figure 3B) and slowed reloading of histones that are displaced (Figure 3B), as well as in disrupted kinetochore organization (Figure 5C). These data are consistent with roles for RSC in both histone removal and reloading. The loss of Isw2p (Figure 6E) also results in slower histone dynamics (Figure 3B), likely due to disrupted reloading of histones. Given that ISW2 is nonessential, other remodeling complexes may contribute to reloading histones at the pericentromere. *ISW2* is known to interact genetically with various components of both the INO80 chromatin-remodeling complex and chromatin assembly complex (Collins *et al.*, 2007; Vincent *et al.*, 2008; Hannum *et al.*, 2009; Costanzo

Nuf2p-GFP for the outer kinetochore. *nps1-105* and *isw2Δ* cells contained either Ame1p-GFP (inner) or Spc24p-GFP (outer). Gal-H3 cells contained either Ndc10p-GFP (inner) or Nuf2p-GFP (outer). The disrupted phenotype observed in the inner kinetochore varied from declustered (*nps1-105*) to a more diffusive cloud (H3 depleted). Asterisks indicate statistically significant differences between sample and corresponding wild-type value (Fisher's exact test, $p < 0.05$; Supplemental Table S4).
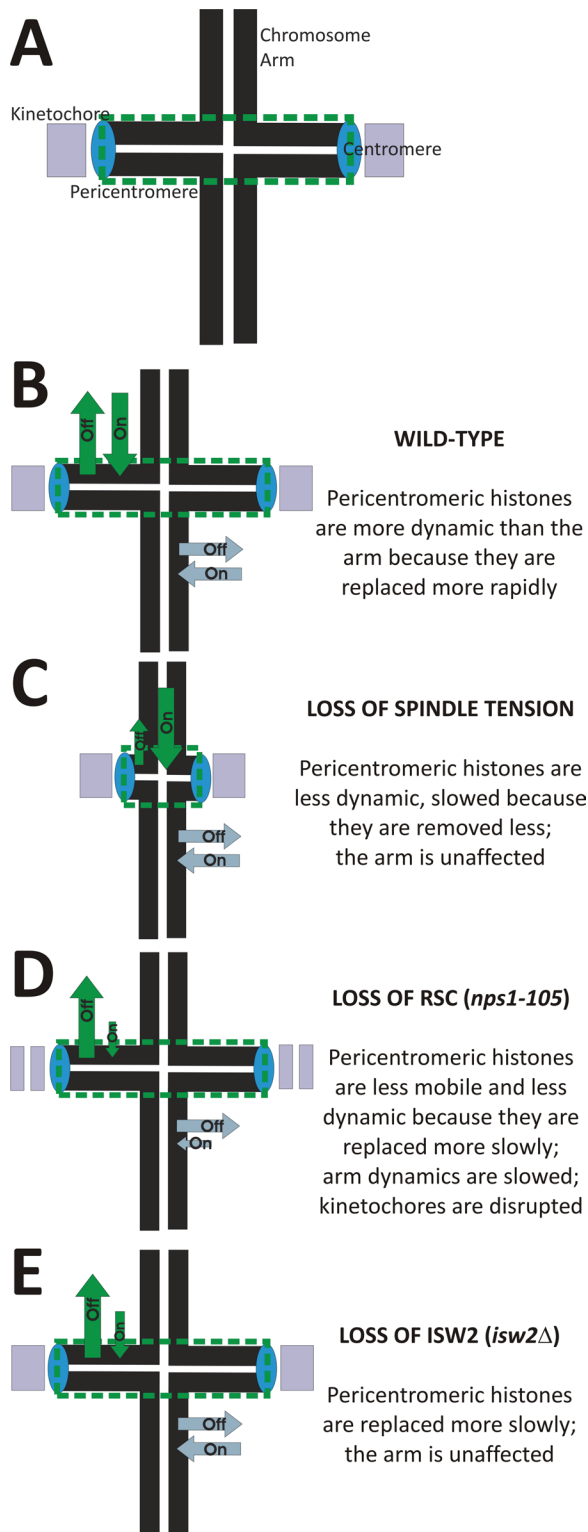
FIGURE 6: Model diagram of histone occupancy in the pericentromere and arm under various experimental conditions. (A) Diagram of replicated bioriented chromosome indicating the locations of the arm and the pericentromere in relation to the centromere and kinetochore. (B) In wild-type cells, histones are more dynamic in the pericentromere than the arm (illustrated by larger arrows at the pericentromere), which is the result of being replaced more rapidly in the pericentromere. Histone on and off rates are balanced (equal-sized arrows) to maintain proper histone occupancy. (C) On loss of spindle tension, histones are not removed as frequently

from pericentromeric chromatin, and the arm is unaffected. (D) Loss of RSC function results in reduced histone dynamics (slower reloading) at the pericentromere and slower histone dynamics throughout the nucleus. Kinetochores appear disrupted due to disturbance of the underlying chromatin structure required for kinetochore organization. (E) Loss of ISW2 results in slower histone dynamics at the pericentromere, likely due to disrupted histone reloading, whereas the chromosome arm is unaffected.

et al., 2010), suggesting possible roles for these remodelers in the maintenance of histone occupancy in the pericentromere. Balanced remodeling at gene promoters is required for maintenance of proper gene expression (Tomar *et al.*, 2009). These experiments demonstrated synthetic lethality between Isw2 and Snf2 of the SWI/SNF chromatin-remodeling complex (*Nps1/Sth1* is a *Snf2* homologue). The remodeling activities of RSC and ISW2 are critical for nucleosome occupancy in the pericentromere while accommodating physical tension.

During chromosome segregation, the mitotic spindle exerts an outward force on the chromosomes that exceeds the amount of force required for nucleosome eviction (Nicklas, 1983, 1988; Mihardja *et al.*, 2006; Yan *et al.*, 2007). We hypothesize that the eviction of nucleosomes under tension serves to equalize the tension across the pericentromeric chromatin. The cell must maintain a balance between nucleosome eviction and reloading to maintain kinetochore organization. Here we provide evidence coupling the imposition of mechanical force (spindle tension) to a distinct chemical reaction to remodel chromatin. Tension sensing is an important component of the spindle-assembly checkpoint, required for preventing aneuploidy and chromosome missegregation (Nicklas *et al.*, 1995; Nicklas, 1997; Biggins and Murray, 2001; Stern and Murray, 2001; Musacchio and Salmon, 2007; Luo *et al.*, 2010). To ensure consistent tension sensing, the chromatin spring must accommodate the fluctuating forces exerted by growing and shortening microtubules without DNA breaks. This consistent tension sensing is accomplished by the balanced off and on rates dictated, at least in part, by RSC and ISW2 chromatin remodeling.

In addition to examining the dynamics of nucleosome turnover in response to tension, this work suggests an ordered sequence of histone removal and deposition (Verreault, 2000; Kimura and Cook, 2001; Akey and Luger, 2003; Jamai *et al.*, 2007). We find that in wild-type cells H2B dynamics are more rapid than those of H4 (Figure 2A). In the absence of tension due to nocodazole treatment, H2B turnover is significantly slower (Figure 3B), and fewer cells exhibit H4 recovery (Figure 3A) in the pericentromere. On repression of an essential kinetochore protein (Gal-*NUF2*), both H2B and H4 dynamics are slowed, and H4 exhibits a lower final percentage recovery, which indicates a lower mobile fraction (Figure 3, B and C). From these data, we hypothesize that the H2A–H2B dimer must be removed to allow for H3–H4 tetramer mobility. This normal sequence of eviction and deposition seems to be abolished in the RSC mutant (*nps1-105*), as H4 turnover is more rapid than that of H2B in the chromosome arm (Figure 3B) and overall dynamics are suppressed in the pericentromere (Figure 3A). We hypothesize that RSC may play a role in directing the ordered remodeling of nucleosomes, and upon loss of RSC activity this stepwise remodeling is abolished. The observed differences in histone dynamics point to an ordered remodeling, which is accomplished in large part by RSC remodeling throughout the nucleus. From these data, we can hypothesize that histone eviction as a result of physical tension occurs in a two-step manner, with H2B being more mobile than H4.

Redefining the pericentromere

This research shows that the pericentromere surrounding the point centromere of budding yeast is functionally distinct from the bulk chromosome arms during mitosis. Traditionally the pericentromere is delineated by histone modifications and variants that result in the unique state of chromatin at the centromere, which has been termed centrochromatin (Sullivan and Karpen, 2004). In addition to histone modifications and variants, the physical state of the chromatin serves to define the pericentromere. Chromatin under tension exhibits a distinct pattern of nucleosome dynamics that might functionally distinguish pericentromeric chromatin during mitosis in budding yeast.

The underlying pericentromeric chromatin is required to form kinetochore–microtubule attachments and maintain kinetochore clustering when under spindle-based tension. The platform on which the kinetochore is built depends on the sequence-specific centromere DNA, as well as on the flanking pericentromeric chromatin. Unlike promoters and repressors that serve as signposts for starting or stopping transcription, the centromere DNA locus forms a node within a larger chromatin network upon which the kinetochore is built. The finding that 55% of the inner kinetochores are disrupted without disruption of the outer kinetochore in H3-repressed cells reveals that the inner kinetochore relies on an intact chromatin foundation. In contrast, the outer kinetochore is less dependent on the underlying chromatin. We propose that the pericentromeric chromatin surrounding a point centromere contributes to the maintenance of kinetochore organization. The structure of the underlying foundation is likely to consist of chromatin meshwork under tension, organized around nodes of Cse4p.

We previously showed that the force produced by the mitotic spindle is not exerted in a linear manner between the sister centromeres (Yeh et al., 2008; Stephens et al., 2011). Instead, the chromatin loops, which are radially dispersed relative to the microtubule spindle axis, provide a vector perpendicular to the site of kinetochore–microtubule attachment and microtubule lengthening and shortening axis. The consequence of this organization is that the chromatin platform occupies a larger area than the sites of microtubule or kinetochore attachment. The organization of the pericentromeric chromatin into a surface platform containing both Cse4p- and H3-containing nucleosomes may be analogous to the organization of chromatin in larger regional centromeres, where a large surface of centromere chromatin is exposed on the surface of the chromosome. It is known that pericentromeric chromatin of regional centromeres is organized into a higher-order structure in which inner kinetochore components (such as CENP-T/W) are known to interact with H3-containing nucleosomes (Marshall et al., 2008; Santaguida and Musacchio, 2009; Ribeiro et al., 2010). The filamentous NDC80 complex connects the inner kinetochore plate to the outer microtubule-binding side of the kinetochore by associating with CENP-T/W via the Mis12 and Knl1 complexes. By building the inner kinetochore on a larger chromatin platform instead of foci of Cse4p, the linkage from the microtubule can be distributed across a larger area of chromatin.

MATERIALS AND METHODS

Yeast strains and imaging

All strains in this study were constructed in the YEF473A background (Bi and Pringle, 1996) unless otherwise noted. Most proteins were tagged with fluorescent proteins through homologous recombination at the C-terminus using PCR-amplified fragments (Joglekar et al., 2009). NUF2-GFP, Gal-NUF2, and Gal-H3 strains were constructed as previously described (Bouck and Bloom, 2005, 2007;

Anderson et al., 2009). Tagging with photoactivatable GFP was performed as previously described (Vorvis et al., 2008).

Yeast strains were grown in 2% glucose, 2% peptone, and 1% yeast extract (YPD) before imaging at 32°C for untreated wild-type and nocodazole-treated cells and 24°C for nps1-105 and isw2Δ strains (Table 1). Overnight cultures were diluted into fresh YPD media several hours before imaging and grown to early to mid logarithmic phase. Unsynchronized cells were washed and imaged on 2% glucose slab media. Nocodazole treatment to depolymerize microtubules was done by adding nocodazole to a final concentration of 20 µg/ml at 1 h before imaging. Gal-H3 cells were depleted of H3 as described (Bouck and Bloom, 2007). Growth in glucose media results in an approximately twofold reduction in nucleosome concentration. Gal-NUF2 strains were grown overnight in 2% galactose, 2% peptone, and 1% yeast extract (YPG) at 24°C to early to mid logarithmic phase. Approximately 1 h before imaging, cells were washed with water and resuspended in YPD at 24°C to repress NUF2 expression. We imaged large-budded cells with shorter spindles, representative of cells arrested due to activation of the spindle assembly checkpoint (Bouck and Bloom, 2005).

Cells were imaged on a wide-field Nikon Eclipse TE2000-U or Nikon FN600 (Nikon, East Rutherford, NJ) microscope stand with a 100× Plan Apo, 1.4 numerical aperture, digital interference contrast oil immersion lens and an Orca ER Camera (Hamamatsu Photonics, Hamamatsu City, Japan). MetaMorph 6.1 (Molecular Devices, Downington, PA) was used to acquire 2 × 2 binned five-plane z-series stacks every 500 nm for FRAP experiments. For characterization of kinetochore organization, unbinned five-plane z-series stacks were acquired, and the brightest (most in-focus) plane was analyzed.

Fluorescence recovery after photobleaching

FRAP experiments were performed by acquiring a z-series in both the GFP and RFP channels before photobleaching. Throughout, a neutral density (ND4) filter was used to reduce photobleaching during photoacquisition. Proteins were photobleached with a single 50-ms pulse of 488-nm laser light focused on the image plane in a diffraction-limited spot. A five-plane z-series of the GFP channel was acquired immediately postbleach and every 20 s for 6 min. After the end of the GFP time lapse, a z-series of the RFP channel was taken to ensure that the cell did not enter anaphase.

The RFP spindle pole bodies were used to determine whether the cells were in metaphase (spindle length between 1.4 and 1.8 µm) and the position of the photobleached region. For nocodazole-treated cells we examined medium-budded cells with fully collapsed spindle pole bodies. To ensure that our analysis in the nps1-105 mutant is also of metaphase cells, we examined spindle pole (Spc29p-RFP) to kinetochore (Ame1p-GFP) distances in both wild-type and nps1-105 cells. On anaphase onset, the distance between the spindle pole and kinetochore is reduced. In wild-type cells this occurred when the spindle was ~1.9–2 µm, and similar values were observed in nps1-105 cells at permissive temperature (Supplemental Figure S3). Therefore we can use the same spindle length criteria (between 1.4 and 1.8 µm) to examine metaphase histone dynamics. Gal-NUF2 cells exhibited a metaphase arrest, so we examined only cells with medium buds, spindles <1.8 µm, and wild-type, roughly circular histone signal (corresponding to preanaphase nuclear shape).

Postacquisition, maximum-projection images were compiled from each z-series at each time point. A 5 × 5 pixel square was drawn over the photobleached region and copied to the RFP image of the spindle pole bodies. The pericentromere was defined by a rectangle corresponding to the region of cohesin enrichment,

Strain number	Genotype	Source
DCB 204	YEF 473a MAT a trp1Δ63 leu2Δ ura3-52 his3Δ200 lys2-801 HHT1ΔTRP1, KAN-GALp-HHT2, NUF2-GFP-URA (using pJK67), SPC29-RFP-Hb	Bouck and Bloom (2007)
DCB 350	YEF 473a MAT a trp1Δ63 leu2Δ ura3-52 his3Δ200 lys2-801 HTB2-GFP-Kan, SPC29-RFP-Hb	Yeh *et al.* (2008)
KBY 2149	YEF 473a MAT a trp1Δ63 leu2Δ ura3-52 his3Δ200 lys2-801 HHT1ΔTRP1, KAN-GALp-HHT2, Ndc10-GFP-URA3 pKK2 *Hind*II cut), SPC29-CFP-HIS3	This study
KBY 8710	YEF 473a MAT a trp1Δ63 leu2Δ ura3-52 his3Δ200 lys2-801 HHF2-GFP-Kan, SPC29-RFP-Hb	This study
KBY 8741	YEF 473a MAT a trp1Δ63 leu2Δ ura3-52 his3Δ200 lys2-801 NPS1-GFP-Kan, SPC29-RFP-Hb	This study
KBY 8743[a]	WHT1a MAT a ade2 ura3 leu2 his3 trp1 nps1-105 AME1-GFP-Kan, SPC29-RFP-Hb	This study
KBY 8745	YEF 473a MAT a trp1Δ63 leu2Δ ura3-52 his3Δ200 lys2-801 AME1-GFP:Kan SPC29-RFP:Hb	This study
KBY 8750	YEF 473a MAT a trp1Δ63 leu2Δ ura3-52 his3Δ200 lys2-801 HTB2-paGFP-Kan, SPC29-RFP-Hb	This study
KBY 8754[a]	WHT1a MAT a ade2 ura3 leu2 his3 trp1 nps1-105 SPC29-RFP-Hb, HTB2-paGFP-Kan	This study
KBY 8760[a]	WHT1a MAT a ade2 ura3 leu2 his3 trp1 nps1-105 Spc24-GFP-Kan, SPC29-RFP-Hb	This study
KBY 8773	YEF 473a MAT a trp1Δ63 leu2Δ ura3-52 his3Δ200 lys2-801 ISW2-GFP-Kan, SPC29-RFP-Hb	This study
KBY 8777	YEF 473a MAT a trp1Δ63 leu2Δ ura3-52 his3Δ200 lys2-801 isw2Δ::Nat, SPC24-GFP-Kan, SPC29-RFP-Hb	This study
KBY 8778	YEF 473a MAT a trp1Δ63 leu2Δ ura3-52 his3Δ200 lys2-801 isw2Δ::Nat, AME1-GFP-Kan, SPC29-RFP-Hb	This study
KBY 8779	YEF 473a MAT a trp1Δ63 leu2Δ ura3-52 his3Δ200 lys2-801 isw2Δ::Nat, HTB2-GFP-Kan, SPC29-RFP-Hb	This study
KBY 8780	YEF 473a MAT a trp1Δ63 leu2Δ ura3-52 his3Δ200 lys2-801 isw2Δ::Nat, HHF2-GFP-Kan, SPC29-RFP-Hb	This study
KBY 8787	YEF 473a MAT a trp1Δ63 leu2Δ ura3-52 his3Δ200 lys2-801 isw2Δ::Nat, HTB2-paGFP-Kan, SPC29-RFP-Hb	This study
KBY 8802[b]	YEF 473a MAT a trp1Δ63 leu2Δ ura3-52 his3Δ200 lys2-801 LEU2-Gal1 Ub-Nuf2, SPC29-RFP-Hb, HTB2-GFP-Kan	This study
KBY 8804[b]	YEF 473a MAT a trp1Δ63 leu2Δ ura3-52 his3Δ200 lys2-801 LEU2-Gal1 Ub-Nuf2, SPC29-RFP-Hb, HHF2-GFP-Kan	This study
MAY 8526	YEF 473a MAT a trp1Δ63 leu2Δ ura3-52 his3Δ200 lys2-801 NUF2-GFP-Kan, SPC29-RFP-Hb	Anderson *et al.* (2009)
WLY 8902[a]	WHT1a MAT a ade2 ura3 leu2 his3 trp1 nps1-105 HTB2-GFP-Kan, SPC29-RFP-Hb	This study
WLY 8903[a]	WHT1a MAT a ade2 ura3 leu2 his3 trp1 nps1-105 HHF2-GFP-Kan, SPC29-RFP-Hb	This study
YWL 492	ura3-52 lys2-801 leu2Δ1 his3Δ200 trp1Δ63 Erg6-PAGFP-Kan	Vorvis *et al.* (2008)

[a]Parent nps1-105 strain from Tsuchiya *et al.* (1998). [b]Parent Gal-Nuf2 strain from Bouck and Bloom (2005).

TABLE 1: *S. cerevisiae* strains.

~800 × 300 nm between the spindle pole bodies (Yeh *et al.*, 2008). The 5 × 5 photobleached region was defined as pericentromeric if more than half of the pixels fell within the cohesin cylinder rectangle dimension (Figure 1).

To calculate $t_{1/2}$ and percentage protein recovery, integrated intensity values were measured at each time point for a 5 × 5 region over the photobleached spot, an unbleached region in the same nucleus, the cell background, and an unbleached cell in the same field of view. These values were further analyzed using Excel (Microsoft, Richmond, WA). We corrected for photobleaching during acquisition by measuring the unbleached intensity over time. The

FRAP rate constant (k) was calculated as follows: $[F_{inf} - F(t)]/[F_{inf} - F(0)] = e^{-kt}$, where F_{inf} is the average fluorescence intensity after maximum recovery, $F(t)$ is the fluorescence intensity at each time point, $F(0)$ is the fluorescence intensity at $t = 0$ s immediately post-bleach, k is the rate constant for exponential decay, and t is time. The $t_{1/2}$ was calculated as $(\ln 2)/k$, and final percentage recovery equals $[F_{inf} - F(0)]/[F_{pre} - F(0)]$.

Samples with a negative percentage recovery were classified as displaying no measurable recovery. The number of samples exhibiting measurable recovery or not was compared with wild-type values by Fisher's exact test of statistical significance. Fisher's exact test is a

statistical significance test used to analyze contingency tables, similar to a chi-squared test, but it allows for smaller sample sizes. Of the cells displaying recovery, further statistical analysis was done using Excel. The upper and lower ranges were calculated as quartile 1 (Q1) − 1.5 × interquartile range (IQR) and Q3 + 1.5 × IQR. Values below or above these limits were defined as outliers. Mean averages and standard deviations of $t_{1/2}$ and percentage recovery were calculated (summarized in Supplemental Tables S1 and S2). To determine whether data sets to be compared had statistically significantly different variances, we first performed an F test ($p < 0.05$). Subsequently, we performed two-tailed Student's t tests (type 2 or 3, depending on F test result) to determine whether the values were statistically significant ($p < 0.05$).

Photoactivation

Similar to the described FRAP technique, photoactivation experiments were performed by acquiring a z-series in both the GFP and RFP channels before photoactivation. A neutral density (ND4) filter was used to reduce photoactivation during photoacquisition. Proteins were photoactivated with one to three 800-ms pulses of 458/10-nm laser light. We also imaged these strains using 405-nm excitation light exciting the full field of view as a control. A z-series of the GFP channel was acquired immediately postbleach and every 15 s for 6 min. After the end of the GFP time lapse, a z-series of the RFP channel was taken to ensure that the cell did not enter anaphase. The RFP spindle pole bodies were used to determine whether the cells were in metaphase (spindle length between 1.4 and 1.8 μm) and the position of the photoactivated region.

For analysis, z-series stacks were compiled into maximum-projection images for each time point. The background intensity value was obtained from the prephotoactivation images. These are defined as the average intensity of a 20 × 20 pixel region plus three SDs. For each postphotoactivation frame, we determined the number of pixels in the region that were brighter than the background value. We then corrected for photoactivation during acquisition by subtracting the average intensity of a 20 × 20 pixel region in an unphotoactivated cell in the same field of view. The corrected number of pixels brighter than background was plotted over time. Proteins were characterized as dispersive or not dispersive based on the slope. Dispersive samples (such as the Erg6p control) exhibited negative slopes, suggesting the spot was getting dimmer over time. Nondispersive samples exhibited a positive slope. The number of samples exhibiting dispersion or not was compared with wild-type values by Fisher's exact test of statistical significance.

REFERENCES

Ahmad K, Henikoff S (2002). The histone variant H3.3 marks active chromatin by replication-independent nucleosome assembly. Mol Cell 9, 1191–1200.

Akey CW, Luger K (2003). Histone chaperones and nucleosome assembly. Curr Opin Struct Biol 13, 6–14.

Anderson M, Haase J, Yeh E, Bloom K (2009). Function and assembly of DNA looping, clustering, and microtubule attachment complexes within a eukaryotic kinetochore. Mol Biol Cell 20, 4131–4139.

Bi E, Pringle JR (1996). ZDS1 and ZDS2, genes whose products may regulate Cdc42p in Saccharomyces cerevisiae. Mol Cell Biol 16, 5264–5275.

Biggins S, Murray AW (2001). The budding yeast protein kinase Ipl1/Aurora allows the absence of tension to activate the spindle checkpoint. Genes Dev 15, 3118–3129.

Bouck DC, Bloom K (2007). Pericentric chromatin is an elastic component of the mitotic spindle. Curr Biol 17, 741–748.

Bouck DC, Bloom KS (2005). The kinetochore protein Ndc10p is required for spindle stability and cytokinesis in yeast. Proc Natl Acad Sci USA 102, 5408–5413.

Cairns BR, Lorch Y, Li Y, Zhang M, Lacomis L, Erdjument-Bromage H, Tempst P, Du J, Laurent B, Kornberg RD (1996). RSC, an essential, abundant chromatin-remodeling complex. Cell 87, 1249–1260.

Cao Y, Cairns BR, Kornberg RD, Laurent BC (1997). Sfh1p, a component of a novel chromatin-remodeling complex, is required for cell cycle progression. Mol Cell Biol 17, 3323–3334.

Chaban Y, Ezeokonkwo C, Chung WH, Zhang F, Kornberg RD, Maier-Davis B, Lorch Y, Asturias FJ (2008). Structure of a RSC-nucleosome complex and insights into chromatin remodeling. Nat Struct Mol Biol 15, 1272–1277.

Chen D, Dundr M, Wang C, Leung A, Lamond A, Misteli T, Huang S (2005). Condensed mitotic chromatin is accessible to transcription factors and chromatin structural proteins. J Cell Biol 168, 41–54.

Cho RJ et al. (1998). A genome-wide transcriptional analysis of the mitotic cell cycle. Mol Cell 2, 65–73.

Clapier CR, Cairns BR (2009). The biology of chromatin remodeling complexes. Annu Rev Biochem 78, 273–304.

Collins SR et al. (2007). Functional dissection of protein complexes involved in yeast chromosome biology using a genetic interaction map. Nature 446, 806–810.

Corona DF, Langst G, Clapier CR, Bonte EJ, Ferrari S, Tamkun JW, Becker PB et al. (1999). ISWI is an ATP-dependent nucleosome remodeling factor. Mol Cell 3, 239–245.

Costanzo M (2010). The genetic landscape of a cell. Science 327, 425–431.

Deal RB, Henikoff JG, Henikoff S (2010). Genome-wide kinetics of nucleosome turnover determined by metabolic labeling of histones. Science 328, 1161–1164.

Desai P, Guha N, Galdieri L, Hadi S, Vancura A (2009). Plc1p is required for proper chromatin structure and activity of the kinetochore in Saccharomyces cerevisiae by facilitating recruitment of the RSC complex. Mol Genet Genomics 281, 511–523.

Dion MF, Kaplan T, Kim M, Buratowski S, Friedman N, Rando OJ (2007). Dynamics of replication-independent histone turnover in budding yeast. Science 315, 1405–1408.

Du J, Nasir I, Benton BK, Kladde MP, Laurent BC (1998). Sth1p, a Saccharomyces cerevisiae Snf2p/Swi2p homolog, is an essential ATPase in RSC and differs from Snf/Swi in its interactions with histones and chromatin-associated proteins. Genetics 150, 987–1005.

Erkina TY, Zou Y, Freeling S, Vorobyev VI, Erkine AM (2010). Functional interplay between chromatin remodeling complexes RSC, SWI/SNF and ISWI in regulation of yeast heat shock genes. Nucleic Acids Res 38, 1441–1449.

Flaus A, Owen-Hughes T (2003). Dynamic properties of nucleosomes during thermal and ATP-driven mobilization. Mol Cell Biol 23, 7767–7779.

Gaber RF, Copple DM, Kennedy BK, Vidal M, Bard M (1989). The yeast gene ERG6 is required for normal membrane function but is not essential for biosynthesis of the cell-cycle-sparking sterol. Mol Cell Biol 9, 3447–3456.

Hannum G, Srivas R, Guenole A, van Attikum H, Krogan NJ, Karp RM, Ideker T (2009). Genome-wide association data reveal a global map of genetic interactions among protein complexes. PLoS Genet 5, e1000782.

Hsu JM, Huang J, Meluh PB, Laurent BC (2003). The yeast RSC chromatin-remodeling complex is required for kinetochore function in chromosome segregation. Mol Cell Biol 23, 3202–3215.

Jackson V (1987). Deposition of newly synthesized histones: new histones H2A and H2B do not deposit in the same nucleosome with new histones H3 and H4. Biochemistry 26, 2315–2325.

Jamai A, Imoberdorf RM, Strubin M (2007). Continuous histone H2B and transcription-dependent histone H3 exchange in yeast cells outside of replication. Mol Cell 25, 345–355.

Jin J, Cai Y, Li B, Conaway RC, Workman JL, Conaway JW, Kusch T (2005). In and out: histone variant exchange in chromatin. Trends Biochem Sci 30, 680–687.

Joglekar AP, Bloom K, Salmon ED (2009). In vivo protein architecture of the eukaryotic kinetochore with nanometer scale accuracy. Curr Biol 19, 694–699.

Kim HJ, Seol JH, Han JW, Youn HD, Cho EJ (2007). Histone chaperones regulate histone exchange during transcription. EMBO J 26, 4467–4474.

Kimura H (2005). Histone dynamics in living cells revealed by photobleaching. DNA Repair (Amst) 4, 939–950.

Kimura H, Cook PR (2001). Kinetics of core histones in living human cells: little exchange of H3 and H4 and some rapid exchange of H2B. J Cell Biol 153, 1341–1353.

Ladoux B, Quivy JP, Doyle P, du Roure O, Almouzni G, Viovy JL (2000). Fast kinetics of chromatin assembly revealed by single-molecule videomicroscopy and scanning force microscopy. Proc Natl Acad Sci USA 97, 14251–14256.

Lee CK, Shibata Y, Rao B, Strahl BD, Lieb JD (2004). Evidence for nucleosome depletion at active regulatory regions genome-wide. Nat Genet 36, 900–905.

Lopes da Rosa J, Holik J, Green EM, Rando OJ, Kaufman PD (2011). Overlapping regulation of CenH3 localization and histone H3 turnover by CAF-1 and HIR proteins in Saccharomyces cerevisiae. Genetics 187, 9–19.

Lorch Y, Maier-Davis B, Kornberg RD (2006). Chromatin remodeling by nucleosome disassembly in vitro. Proc Natl Acad Sci USA 103, 3090–3093.

Luger K, Mader AW, Richmond RK, Sargent DF, Richmond TJ (1997). Crystal structure of the nucleosome core particle at 2.8 A resolution. Nature 389, 251–260.

Luo J, Xu X, Hall H, Hyland EM, Boeke JD, Hazbun T, Kuo MH (2010). Histone H3 exerts a key function in mitotic checkpoint control. Mol Cell Biol 30, 537–549.

Marshall OJ, Marshall AT, Choo KH (2008). Three-dimensional localization of CENP-A suggests a complex higher order structure of centromeric chromatin. J Cell Biol 183, 1193–1202.

Mihardja S, Spakowitz AJ, Zhang Y, Bustamante C (2006). Effect of force on mononucleosomal dynamics. Proc Natl Acad Sci USA 103, 15871–15876.

Musacchio A, Salmon ED (2007). The spindle-assembly checkpoint in space and time. Nat Rev Mol Cell Biol 8, 379–393.

Nicklas RB (1983). Measurements of the force produced by the mitotic spindle in anaphase. J Cell Biol 97, 542–548.

Nicklas RB (1988). The forces that move chromosomes in mitosis. Annu Rev Biophys Biophys Chem 17, 431–449.

Nicklas RB (1997). How cells get the right chromosomes. Science 275, 632–637.

Nicklas RB, Ward SC, Gorbsky GJ (1995). Kinetochore chemistry is sensitive to tension and may link mitotic forces to a cell cycle checkpoint. J Cell Biol 130, 929–939.

Parnell TJ, Huff JT, Cairns BR (2008). RSC regulates nucleosome positioning at Pol II genes and density at Pol III genes. EMBO J 27, 100–110.

Pusarla RH, Bhargava P (2005). Histones in functional diversification. Core histone variants. FEBS J 272, 5149–5168.

Ribeiro SA, Vagnarelli P, Dong Y, Hori T, McEwen BF, Fukagawa T, Flors C, Earnshaw WC (2010). A super-resolution map of the vertebrate kinetochore. Proc Natl Acad Sci USA 107, 10484–10489.

Saha A, Wittmeyer J, Cairns BR (2002). Chromatin remodeling by RSC involves ATP-dependent DNA translocation. Genes Dev 16, 2120–2134.

Santaguida S, Musacchio A (2009). The life and miracles of kinetochores. EMBO J 28, 2511–2531.

Saunders MJ, Yeh E, Grunstein M, Bloom K (1990). Nucleosome depletion alters the chromatin structure of Saccharomyces cerevisiae centromeres. Mol Cell Biol 10, 5721–5727.

Schwabish MA, Struhl K (2004). Evidence for eviction and rapid deposition of histones upon transcriptional elongation by RNA polymerase II. Mol Cell Biol 24, 10111–10117.

Smith S, Stillman B (1991). Stepwise assembly of chromatin during DNA replication in vitro. EMBO J 10, 971–980.

Stephens AD, Haase J, Vicci L, Taylor RM, Bloom K (2011). Cohesin, condensin, and the intramolecular centromere loop together generate the mitotic chromatin spring. J Cell Biol 193, 1167–1180.

Stern BM, Murray AW (2001). Lack of tension at kinetochores activates the spindle checkpoint in budding yeast. Curr Biol 11, 1462–1467.

Sullivan BA, Karpen GH (2004). Centromeric chromatin exhibits a histone modification pattern that is distinct from both euchromatin and heterochromatin. Nat Struct Mol Biol 11, 1076–1083.

Thiriet C, Hayes JJ (2005). Replication-independent core histone dynamics at transcriptionally active loci in vivo. Genes Dev 19, 677–682.

Tomar RS, Psathas JN, Zhang H, Zhang Z, Reese JC (2009). A novel mechanism of antagonism between ATP-dependent chromatin remodeling complexes regulates RNR3 expression. Mol Cell Biol 29, 3255–3265.

Tsuchiya E, Hosotani T, Miyakawa T (1998). A mutation in NPS1/STH1, an essential gene encoding a component of a novel chromatin-remodeling complex RSC, alters the chromatin structure of Saccharomyces cerevisiae centromeres. Nucleic Acids Res 26, 3286–3292.

Tsuchiya E, Uno M, Kiguchi A, Masuoka K, Kanemori Y, Okabe S, Mikayawa T (1992). The Saccharomyces cerevisiae NPS1 gene, a novel CDC gene which encodes a 160 kDa nuclear protein involved in G2 phase control. EMBO J 11, 4017–4026.

Tsukiyama T, Palmer J, Landel CC, Shiloach J, Wu C (1999). Characterization of the imitation switch subfamily of ATP-dependent chromatin-remodeling factors in Saccharomyces cerevisiae. Genes Dev 13, 686–697.

Verreault A (2000). De novo nucleosome assembly: new pieces in an old puzzle. Genes Dev 14, 1430–1438.

Vignali M, Hassan AH, Neely KE, Workman JL (2000). ATP-dependent chromatin-remodeling complexes. Mol Cell Biol 20, 1899–1910.

Vincent JA, Kwong TJ, Tsukiyama T (2008). ATP-dependent chromatin remodeling shapes the DNA replication landscape. Nat Struct Mol Biol 15, 477–484.

Vorvis C, Markus SM, Lee WL (2008). Photoactivatable GFP tagging cassettes for protein-tracking studies in the budding yeast Saccharomyces cerevisiae. Yeast 25, 651–659.

Whitehouse I, Rando OJ, Delrow J, Tsukiyama T (2007). Chromatin remodelling at promoters suppresses antisense transcription. Nature 450, 1031–1035.

Whitehouse I, Stockdale C, Flaus A, Szczelkun MD, Owen-Hughes T (2003). Evidence for DNA translocation by the ISWI chromatin-remodeling enzyme. Mol Cell Biol 23, 1935–1945.

Widmer RM, Lucchini R, Lezzi M, Meyer B, Sogo JM, Edstrom JE, Koller T (1984). Chromatin structure of a hyperactive secretory protein gene (in Balbiani ring 2) of Chironomus. EMBO J 3, 1635–1641.

Xue Y, Canman JC, Lee CS, Nie Z, Yang D, Moreno GT, Young MK, Salmon ED, Wang W (2000). The human SWI/SNF-B chromatin-remodeling complex is related to yeast rsc and localizes at kinetochores of mitotic chromosomes. Proc Natl Acad Sci USA 97, 13015–13020.

Yan J, Maresca TJ, Skoko D, Adams CD, Xiao B, Christensen MO, Heald R, Marko JF (2007). Micromanipulation studies of chromatin fibers in Xenopus egg extracts reveal ATP-dependent chromatin assembly dynamics. Mol Biol Cell 18, 464–474.

Yeh E, Haase J, Paliulis LV, Joglekar A, Bond L, Bouck D, Salmon ED, Bloom KS (2008). Pericentric chromatin is organized into an intramolecular loop in mitosis. Curr Biol 18, 81–90.